12th International Symposium on Turbulence and Shear Flow Phenomena (TSFP12)
Osaka, Japan (Online), July 19-22, 2022

FLOW PAST AN INCLINED SPHEROID IN HOMOGENEOUS AND STRATIFIED ENVIRONMENTS

Sheel Nidhan
Mechanical and Aerospace Engineering
University of California San Diego
CA 92093
snidhan@ucsd.edu

Jose L. Ortiz-Tarin
Mechanical and Aerospace Engineering
University of California San Diego
CA 92093
jlortiztarin@gmail.com

Sutanu Sarkar
Mechanical and Aerospace Engineering
University of California San Diego
CA 92093
sarkar@ucsd.edu

ABSTRACT

Large eddy simulations (LES) are performed to study the flow past a 6:1 prolate spheroid placed at an angle of incidence of $\alpha = 10^\circ$. The diameter-based Reynolds number ($Re = U_\infty D/\nu$) is set to a value of 5×10^3 and four values of diameter-based Froude numbers ($Fr = U_\infty/ND$) are analyzed: $Fr = \infty, 6, 1.9$, and 1. Visualizations of coefficient of pressure (C_p) and friction (C_f) contours reveal asymmetry in the $Fr = \infty$ and 6 flows while, at $Fr = 1$ and $Fr = 1.9$, the flow over body does not have any visible asymmetry. This finding is further corroborated through the analysis of force coefficients on the body. The changes in the pressure coefficients (C_p), friction coefficients (C_f), and drag coefficients (C_d) with the Froude number are described in detail for $\alpha = 10^\circ$. We also present the analyses of forces on the body at $\alpha = 0^\circ$ angle of incidence for comparison with the $\alpha = 10^\circ$ cases.

INTRODUCTION

Despite their widespread presence in applications, slender body flows have received significantly less attention compared to the flows past bluff bodies. There are some particularities that make the study of slender body flows especially challenging. In a numerical simulation, resolving the boundary layer (BL) of a long body is computationally more expensive than resolving the BL of a blunt body. Additionally, in experimental studies, slender bodies can take up a significant portion of the measurement section and, since they normally generate thin wakes, they are potentially harder to probe and measure.

The first experimental study of flow past a slender body dates back to Chevray (1968) who investigated the wake of a 6:1 prolate spheroid at $Re = 4.5 \times 10^5$. The wake measurements spanned a streamwise distance of $x/D = 18$. Han & Patel (1979) conducted an experimental study of flow past a 4.3:1 spheroid at different angles of incidence (α) at $Re \approx 2 \times 10^4$. They primarily focused on the flow separation pattern, identifying two regimes as α was changed: (i) closed or bubble separation and (ii) open or free-vortex type separation. Wang *et al.* (1990) extended the study of Han & Patel (1979) to prolate spheroids with aspect ratios of 2:1, 3:1, and 4:1 for a wide range of α in the range $[0^\circ, 90^\circ]$. Experimental studies have also been performed at higher Re with tripped BL by Fu *et al.* (1994) and Chesnakas & Simpson (1994). Jiménez *et al.* (2010) and Ashok *et al.* (2015*a*) studied the high Re wake of a DARPA SUBOFF at $\alpha = 0^\circ$ and in pitch configurations, respectively. While Jiménez *et al.* (2010) focused on the self-similarity and scalings in the near to intermediate wake, Ashok *et al.* (2015*a*) characterized the wake asymmetries induced due to the pitch configuration.

Numerical simulations have also been used to study slender body flows. Constantinescu *et al.* (2002) and Wikström *et al.* (2004) conducted RANS and LES studies of flow past a 6:1 prolate spheroid at $Re = 4.2 \times 10^6$ and $\alpha = 10^\circ$, 20°. Tezuka & Suzuki (2006) carried out a three-dimensional stability analysis study for the flow past a 4:1 spheroid for varying α. For $\alpha \neq 0^\circ$, as Re was increased, they found transition from a symmetric to an asymmetric flow configuration in the longitudinal center-plane. The flow asymmetry at nonzero angle of incidence was later studied in more detail using DNS by Jiang *et al.* (2015). In the last few years, the wake of a DARPA SUBOFF has also been studied through LES by Posa & Balaras (2016); Kumar & Mahesh (2018) at $Re \sim O(10^5)$. Ortiz-Tarin *et al.* (2021) was the first study of an unstratified slender body flow that probed far wake statistics, extending to $x/D = 80$.

The LES study by Ortiz-Tarin *et al.* (2019) is the first to take background stratification into account for the study of slender body flows. Their high-resolution LES study was conducted for a 4:1 spheroid at zero angle of attack, $Re = 10^4$ and $Fr = \infty, 3, 1$ and 0.5. They analyzed the laminar BL evolution, force distribution, and the near- and far-field characteristics of the steady lee waves. In the current work, we build upon their work studying the effect of varying Fr on the flow past a 6:1 spheroid placed at a moderate angle of incidence ($\alpha = 10^\circ$). We analyze the effect of stratification on: (i) the variation of C_p, C_f, (ii) the forces on the body, and (iii) the flow separation. We also present a brief analysis of forces on the body at $\alpha = 0^\circ$ for comparison with $\alpha = 10^\circ$ cases. To the best of our knowledge, this is the first study exploring the flow characteristics of an inclined slender body flow in stratified environments. In future work, we plan to extend this study to the analysis of vorticity and wake dynamics in these flows.

NUMERICAL METHODOLOGY

The numerical solver used for these simulations have been extensively validated in the past for body-inclusive simulations of stratified wakes (Ortiz-Tarin *et al.*, 2019; Chongsiripinyo & Sarkar, 2019; Ortiz-Tarin *et al.*, 2021; Nidhan *et al.*, 2019, 2020, 2022). For a detailed description of the solver, boundary conditions and immersed boundary method (IBM) approach, we refer the interested readers to Chongsiripinyo & Sarkar (2019).

In the present work, $Re = 5 \times 10^3$ and four different $Fr = \infty, 6, 1.9$, and 1 are simulated for two angles of incidence $\alpha = 0^\circ$ and 10°. For the stratified cases at $\alpha = 10^\circ$, radial and streamwise domains span $0 \le r/D \le 53$ and $-30 \le x/D \le 50$, respectively. A large radial extent together with a sponge layer on the boundaries weaken the IGWs before they hit the end of the computational domain and hence control the amplitude of spurious reflected waves. Numbers of grid points in different directions are as follows: $N_r = 1000$ in the radial direction, $N_\theta = 128$ in the azimuthal direction, and $N_x = 3584$ in the streamwise direction. For the unstratified wake at $\alpha = 10^\circ$, radial and streamwise domains span $0 \le r/D \le 21$ and $-11 \le x/D \le 47$ while $N_r = 718, N_\theta = 256$, and $N_x = 2560$. At $\alpha = 0^\circ$, we simulate the wakes till a downstream distance of $x/D = 30$ and up to $r/D = 17$ and 53 for unstratified and stratified cases, respectively. The grid point distribution for $\alpha = 0^\circ$ cases are as follows: $N_r = 1000$ and 910 for stratified and unstratified cases, respectively, $N_\theta = 128$, and $N_x = 3584$.

BODY FORCES AT $\alpha = 0^\circ$

Figure 1(a) and (b) show the variation of the pressure coefficient $C_p = (P - P_\infty)/0.5\rho U_\infty^2$ and skin-friction coefficient $C_f = Re^{0.5}|\tau_x|/0.5\rho U_\infty^2$, respectively, for different values of Fr at $\alpha = 0^\circ$. In the reported C_f, the raw skin friction coefficient is multiplied by $Re^{0.5}$ to obtain an $O(1)$ value. The $\theta = 0^\circ$ and 90° labels correspond to the horizontal $x-y$ and vertical $x-z$ plane, respectively. An averaging time window of $30D/U_\infty$ is used to obtain these results.

For $Fr \ge 1.9$ cases (figure 1(a)), the drop of pressure and its recovery primarily occur towards the beginning and the end of the body, respectively. For $-2 \lessapprox x/D \lessapprox 1$, C_p remains approximately constant for $Fr \ge 1.9$. On the other hand, C_p in $Fr = 1$ case shows a monotonic decay till $x/D \approx 2$ and a slight recovery for $x/D \gtrapprox 2$, indicating strong effect of buoyancy on the flow over the body. For $Fr \ge 1.9$, C_p variations are qualitatively very similar. The differences between $Fr = \infty$ and the critical Fr_c curves are less pronounced in the 6:1 spheroid ($Fr_c = 1.9$) than what was observed in the 4:1 spheroid ($Fr_c \approx 1$) as reported by Ortiz-Tarin *et al.* (2019). Anisotropy between horizontal and vertical plane C_p curves appears at $Fr = 1.9$ and increases slightly at $Fr = 1$. Pressure visualizations (not shown here) confirm that the low pressure region in the tail of the spheroid (in the vertical plane) at $Fr = 1$ is imposed by the steady lee-wave field, indicating a strong influence of buoyancy on the flow at this value of Fr.

Figure 1(b) shows the variation of C_f for different Fr at $\alpha = 0^\circ$. Similar to the behavior of C_p, the variation of C_f for $Fr = 6$ and ∞ are very similar. The flow separates at $x/D = 2.34$ for the unstratified flow (marked by $C_f \to 0$). This value is in excellent agreement with the result of Patel & Kim (1994). $Fr = 1.9$ shows elevated and suppressed levels of C_f in vertical and horizontal planes, respectively, compared to $Fr = 6$ and ∞. At $Fr = 1$, C_f in the vertical plane further increases compared to $Fr = 1.9$. Moreover, in the horizontal plane as well, $Fr = 1$ shows higher C_f than $Fr = \infty$ and 6 for $x/D \gtrapprox 0.5$. Increased C_f in the vertical plane for $Fr = 1$ and 1.9 is a consequence of thinner BL over the body (not shown here for brevity) compared to $Fr = 6$ and ∞. In the horizontal plane, for $Fr = 1$ (compared to $Fr = \infty$), BL thickens between $x/D \approx -2$ to 0 and gets thinner beyond $x/D \approx 1$, explaining the trend of C_f in the horizontal plane for $Fr = 1$.

$\alpha = 0^\circ$, Fr	C_d	C_d^f	C_d^p	$\Delta C_d = C_d - C_d(\infty)$
$Fr = \infty$	0.24	0.22	0.02	0
$Fr = 6$	0.26	0.23	0.03	0.02
$Fr = 1.9$	0.32	0.25	0.07	0.08
$Fr = 1$	0.52	0.29	0.23	0.28

Table 1: Drag coefficients (C_d) and corresponding pressure (C_d^p) and friction contributions (C_d^f) for $\alpha = 0^\circ$ at different Fr.

Table 1 presents $C_d = F_d/(0.5\rho_o U_\infty^2 A)$ for different Fr at $\alpha = 0^\circ$. Here, $A = \pi D^2/4$. There is a monotonic increase in C_d, C_d^p, and C_d^f with increasing stratification levels. Friction contributes more to the drag than pressure (except at $Fr = 1$), as expected for a slender body flow. However, compared to flow past a 4:1 spheroid (Ortiz-Tarin *et al.*, 2019), we find that the effect of stratification on the overall drag, quantified by $\Delta C_d = C_d - C_d(\infty)$, is weaker in the 6:1 spheroid. Between $Fr = \infty$ and $Fr = 1.9$, C_d changes by $\approx 33\%$ in the present case while there was a 100% increase in the 4:1 spheroid. This smaller increase in C_d for 6:1 spheroid is primarily due to a smaller increase in C_d^p at $Fr_c = 1.9$ (compared to $Fr = \infty$), unlike in the 4:1 prolate spheroid. It is only when $Fr = 1$ that we see a sharp jump in C_d^p leading to a $\approx 100\%$ increase in C_d, consistent with the differences we observe in C_p curves (figure 1a) between $Fr = 1$ and $Fr \ge 1.9$ cases.

It is a well-established observation that the amplitude of steady lee-waves decreases with increasing value of Fr in the $Fr \ge 1$ regime for a variety of wake generators, including 6:1 prolate spheroid (Bonneton *et al.*, 1993; Meunier *et al.*, 2018). Specifically, Meunier *et al.* (2018) found that the lee-wave amplitude for a 6:1 spheroid (based on $\partial w/\partial z$) decayed as Fr^{-2}. On the other hand, it should be noted that the definition of critical Fr_c given by Ortiz-Tarin *et al.* (2019) is based purely on kinematic considerations, i.e., by equating half-wavelength of the lee-wave to the length of the body. As a result, $Fr_c = L/\pi D$ increases linearly with the aspect ratio. Thus, for the 6:1 spheroid, we see a weaker effect of stratification on the drag at its critical value of $Fr_c = 6/\pi = 1.9$ compared to the 4:1 spheroid for which $Fr_c = 4/\pi = 1.27$ is lower. That the lee wave field in the $Fr = 1.9$ case is weaker than in the $Fr = 1$ case is also confirmed also by quantification of the pressure field, not shown here for brevity.

BODY FORCES AT $\alpha = 10^\circ$

Introducing even a moderate angle of incidence, namely $\alpha = 10^\circ$, significantly changes the characteristics of flow on the body, reflected by significantly different trends of C_p, C_f and force coefficients in $\alpha = 10^\circ$ flows compared to their $\alpha = 0^\circ$ counterparts. In what follows, we discuss the trends of above-mentioned quantities when $\alpha = 10^\circ$ and $Fr = \infty, 6, 1.9$, and 1. For $\alpha = 10^\circ$, a time averaging window of approximately $50D/U_\infty$ is used.

Coefficient of Pressure C_p

Figure 2(a-h) show the pressure contours on the leeside and windside of the body. We also present the variation of C_p along $y = 0$ line on the leeside and windside in figure 2(i,j),

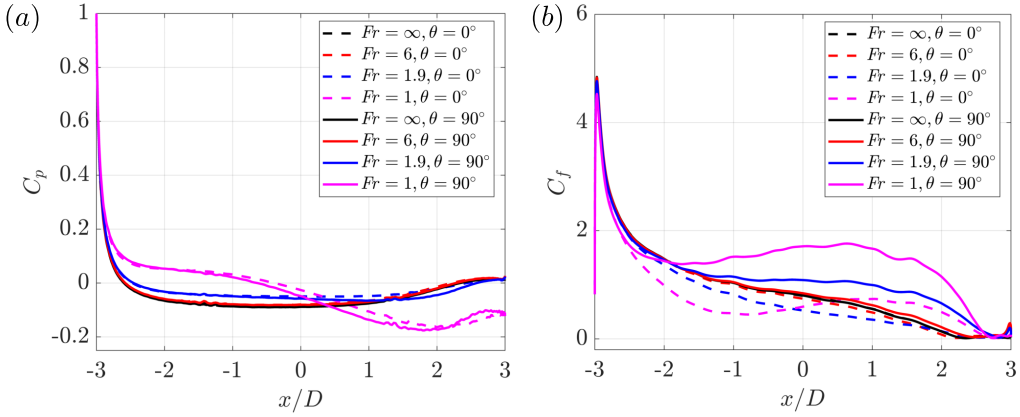

Figure 1: Variation of (a) pressure coefficient C_p and (b) skin-friction coefficient C_f for different Fr at zero angle of attack ($\alpha = 0°$). The $\theta = 0°$ and 90° curves correspond to variations on the surface in the horizontal ($\theta = 0°$) plane and the vertical ($\theta = 90°$) planes on the spheroid. Plotted value of C_f is $Re^{0.5}$ times the friction coefficient.

respectively. C_p obtained from potential flow solution is also presented for comparison in figure 2(i,j). On both sides, the agreement between the potential solutions and LES simulations is excellent till $x/D \approx 1$. Beyond $x/D \approx 1$ LES simulations deviate from potential solutions, presumably due to the three-dimensionality of BL evolution and effects of flow separation. Pressure drop on both sides primarily happens near to the nose of the body and in the ascending order of Fr, i.e., the pressure drop in the nose for $Fr = 1 > 1.9 > 6 > \infty$ (figure 2(i)). It is also worth noting that the $Fr = 6$ and ∞ cases show asymmetry in the leeside pressure contours about the $y = 0$ plane as shown in figure 2(a,c).

On the leeside, for $Fr \geq 1.9$ cases, pressure recovers continuously, albeit slowly, after the initial drop in the nose (figure 2i). On the contrary, pressure in the $Fr = 1$ case, which shows the lowest initial drop (from the stagnation value at the nose) of all cases in the fore of the body ($x/D < 0$) drops below that of the remaining cases for $x/D > 0$. This is evident both from contours (figure 2g) and C_p plots (figure 2i). Mean pressure contours in the vicinity of the spheroid (not shown here for brevity), reveal a strong low-pressure region on the entirety of the leeside. This low-pressure region is imposed by the steady lee wave field at $Fr = 1$. The differences between the unstratified case and strongly stratified cases ($Fr = 1.9$ and 1) are even more pronounced on the windside compared to the leeside of the spheroid. Beyond $x/D \approx 2$, C_p of $Fr = 1.9$ and 1 fall significantly below those of $Fr = \infty$ and 6 (figure 2j), followed by a sharp recovery towards the end. The contours in figure 2(b,d,f,h) confirm this trend of higher and lower pressure at the head and tail, respectively, for the $Fr = 1$ and 1.9 cases compared to $Fr \geq 6$.

Coefficient of Friction C_f

Figure 3(a-h) show the contours of scaled shear stress $Re^{0.5}|\tau_x|$ on the leeside (left) and windside (right) for all cases at $\alpha = 10°$. In figure 3(i,j), we present the variation of C_f on the spheroid surface and in the $y = 0$ plane on both sides. Similar to the pressure contours, a distinct asymmetry is present on the leeside of $Fr = \infty$ and 6 flows as shown figure 3(a,c), to be discussed in more detail in the next subsection.

The shear stress contours show that flow separation primarily happens on the leeside at $\alpha = 10°$ across all Fr. The region of separated flow can be identified by the region of $|\tau_x| \to 0$, marked in green in figure 3 contours. For $Fr = \infty$ and 6, flow separates primarily from the two lateral sides on the lee of the body (figure 3(a,c)). There is a central region near $y = 0$ which remains attached until nearly the tail. In the $Fr = 1.9$ case, separation occurs from the sides as well as the central region around the $y = 0$ plane (figure 3e) while in the $Fr = 1$ case, separation primarily happens in the central region (figure 3g) and not at the sides. Thus, it can be inferred that the stratification level strongly influences the flow separation even at the moderate non-zero angles of attack of this study.

In the vertical-center plane ($y = 0$), C_f varies similarly for all Fr on both sides (figure 3(i,j)) till $x/D \approx 0$. On the leeside (figure 3i) and for $x/D \geq 0$, the $Fr = \infty$ and 6 cases show higher C_f than the strongly stratified cases of $Fr = 1.9$ and 1. On the windside, beyond $x/D \approx 1$, $Fr \leq 1.9$ cases show elevated C_f as compared to $Fr \geq 6$ (figure 3j). This region of elevated surface shear in the $Fr = 1.9$ and 1 flows coincides with the region of steep pressure drop observed at $x/D > 1$ (figure 2j).

Force Coefficients

Figure 4(a,b,c) present the force coefficients ($C_i = F_i/0.5\rho U_\infty^2 A$) at $\alpha = 10°$, decomposed between pressure and friction contributions. Here C_x, C_y and C_z correspond to drag (C_d), lateral force, and lift (C_l) on the body, respectively. We first discuss C_d and C_l and follow by noting the unusual characteristics of C_y for $\alpha = 10°$. Figure 4(d) also shows C_d for $\alpha = 0°$ for reference. In $\alpha = 0°$ cases, $C_l \approx 0$ and $C_y \approx 0$ at all Fr indicating no asymmetry in the flow over body.

For all Fr, C_d, C_d^f and C_d^p (figure 4a) at $\alpha = 10°$ increase relative to the zero degree angle of incidence ((figure 4d). Similar to $\alpha = 0°$, there is a weak monotonic increase in C_d till $Fr = 1.9$ and a large jump thereafter at $Fr = 1$. This jump primarily comes from an approximately 100% increase in C_d^p from $Fr = 1.9$ to $Fr = 1$. Figure 2(g,h) show that the pressure contours at $Fr = 1$ are quite different from those of $Fr \geq 1.9$. The tail and nose on the leeside and windside, respectively, are at a lower and higher pressure (compared to $Fr \geq 1.9$ cases) which leads to an enhanced C_d^p. For C_l, primary contributor is the pressure rather than shear, as expected for a moderate angle of incidence. It is interesting to note that C_l decreases till $Fr = 1.9$ and then increases significantly at $Fr = 1$ case, resulting from an increase in C_l^p. The reason for this increase is the large difference between the leeside and windside pressure in $Fr = 1$ flow as shown in figure 2(g,h).

Figure 4(c) shows that $C_y \neq 0$ for $Fr = \infty$ and 6 at $\alpha = 10°$. For $Fr = \infty$, $C_y \approx -0.05$ and for $Fr = 6$, $C_y \approx 0.05$. This value is approximately 12% of the streamwise drag force

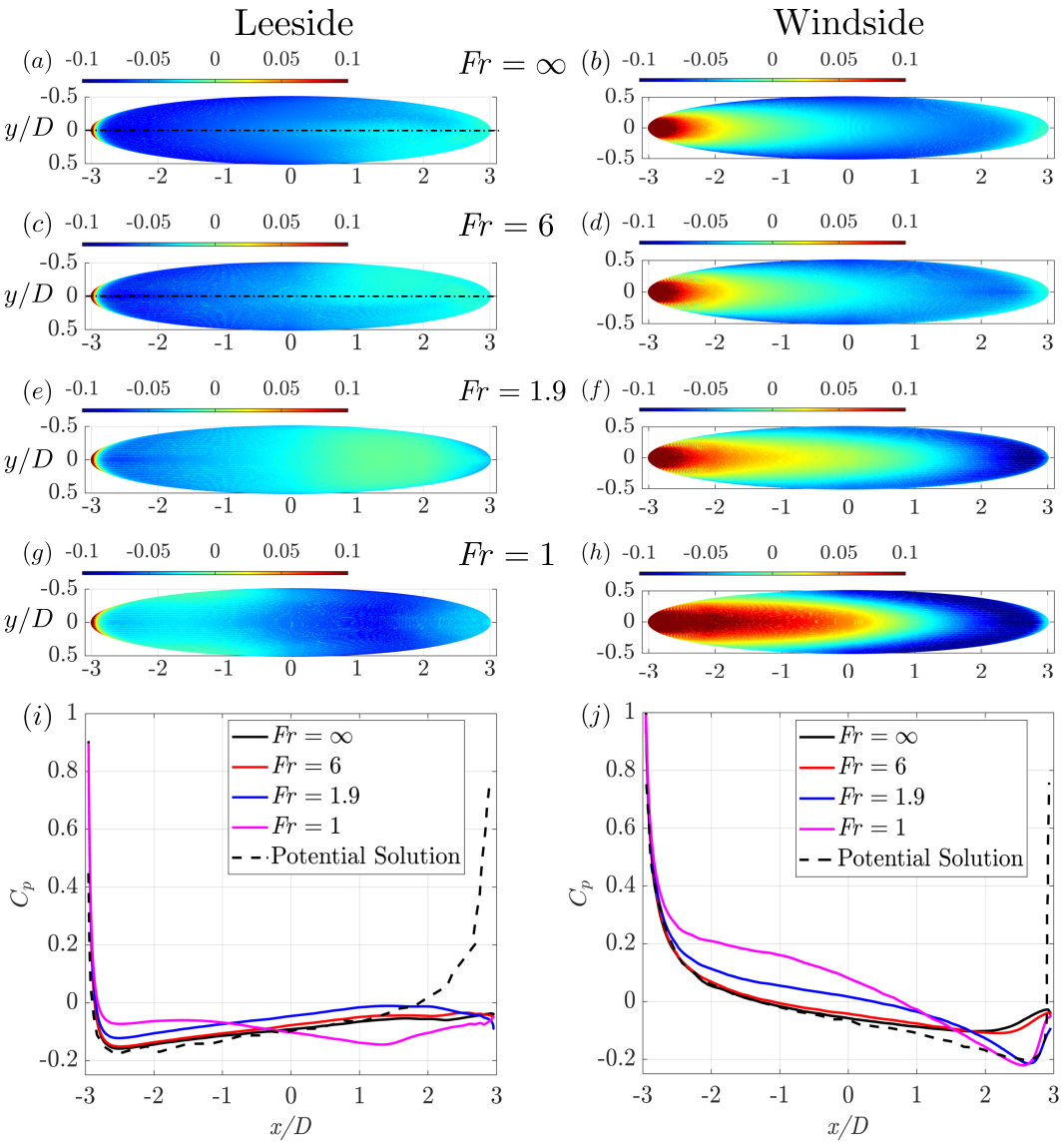

Figure 2: Pressure contours on the leeside (a,c,e) and windside (b,d,f) of the spheroid shown for all simulated Fr at $\alpha = 10°$. Dashed lines in (a) and (c) correspond to $y = 0$. Also shown is the variation of C_p (i, j) on the leeside and windside of the body surface in the $y = 0$ plane. Potential solution for C_p is also shown in dashed line, obtained from Piquet & Queutey (1992).

in both cases. Intuitively, C_y should be equal to zero due to reflectional symmetry in the configuration about the $y = 0$ plane. Non-zero C_y implies lateral asymmetry in the flow on the body. Pressure and friction contours in figure 2(a,c) and 3(a,c), respectively, show that this is indeed the case and the asymmetry originates on the leeside of the body at $x/D \gtrapprox 1$ (the $y = 0$ intersection of the body surface is shown to better identify this lateral asymmetry). No asymmetry is present on the windside flow over the spheroid. When the value of Fr is decreased to 1.9, $C_y \to 0$. Further decrease to $Fr = 1$ also results in $C_y = 0$. This indicates that the flow asymmetry is suppressed as the stratification is increased. Figure 2(e,g) and figure 3(e,g) also confirm that for $Fr = 1.9$ and 1, no asymmetry is visually evident on the leeside of the spheroid. Hence, two important findings from the analysis of C_y are: (i) the weakly stratified ($Fr = 6$) and unstratified ($Fr = \infty$) flow exhibit lateral asymmetry and (ii) this asymmetry is suppressed as the strength of stratification is increased, i.e., at $Fr = 1.9$ and 1.

Our finding regarding lateral asymmetry in the unstratified case is in accord with previous studies on flow past slender bodies (Tezuka & Suzuki, 2006; Ashok *et al.*, 2015*a*,*b*; Jiang *et al.*, 2015). It is also interesting to note that the C_y of $Fr = \infty$ and $Fr = 6$ are similar in magnitude but flipped in sign. We hypothesize that the $Fr = \infty$ and $Fr = 6$ flows might be locked in two different reflectional-symmetry-breaking states, with each state being equally probable. There can be a switching between these two states at a very large timescale. The existence of a long time scale for switching between different reflection-symmetry-breaking states have been extensively researched in flow past three-dimensional blunt bodies (Grandemange *et al.*, 2013; Rigas *et al.*, 2014; Dalla Longa *et al.*, 2019). Interestingly, Jiang *et al.* (2015), who also found lateral asymmetry in their flow (6:1 spheroid at $\alpha = 45°$), did not find a switch even after $600D/U_\infty$. We aim to investigate the characteristics of the intermediate to far wake, besides looking at near-body flow. Hence, running the simulations for $T \sim 1000D/U_\infty$ would be prohibitively expensive and out of scope of the current work.

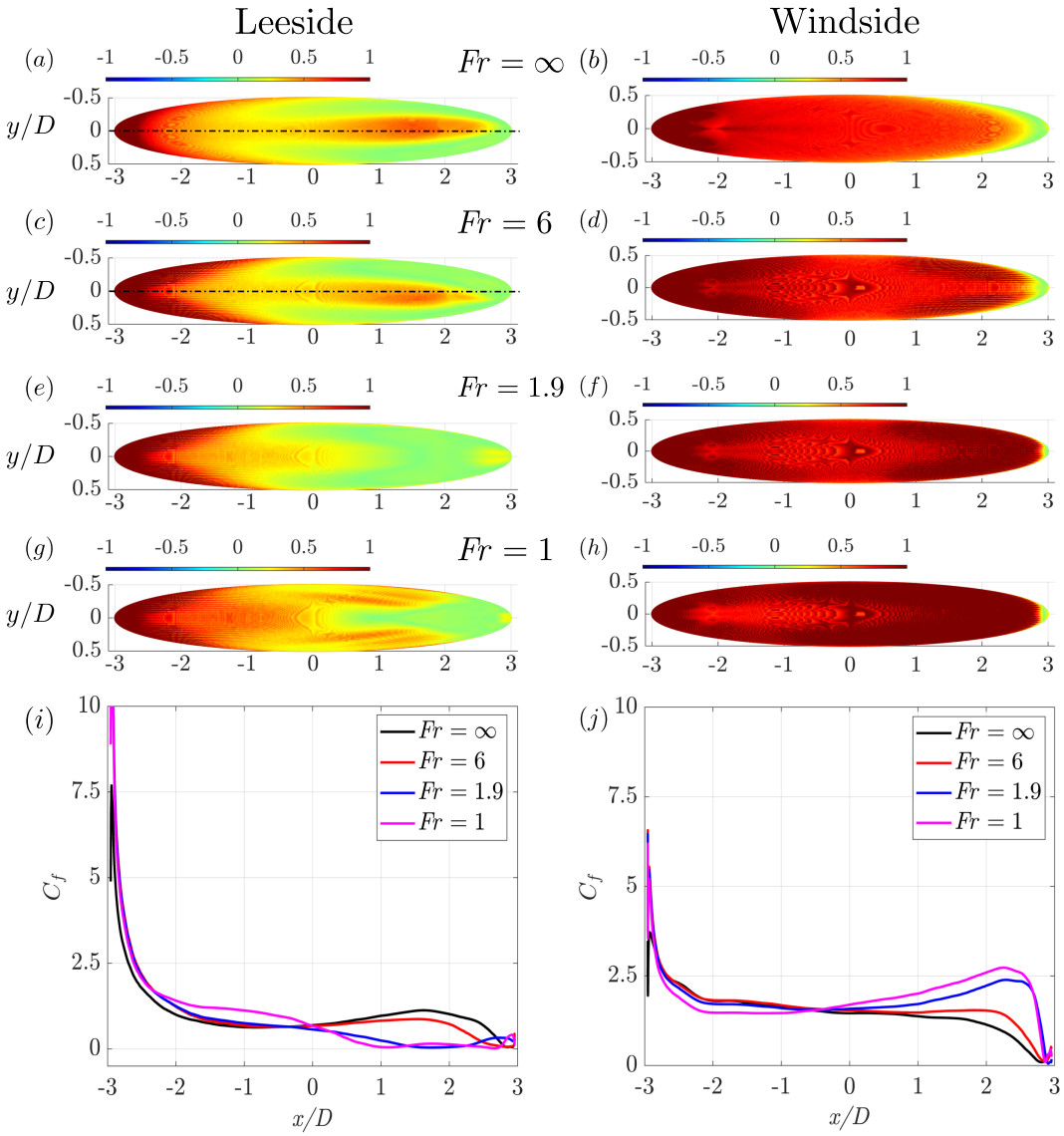

Figure 3: Contours of $Re^{0.5}|\tau_x|$ (a-h) on the leeside and windside of the spheroid for all Fr at $\alpha = 10°$. Dashed lines in (a) and (c) correspond to $y = 0$. Variation of C_f (i, j) on the leeside and windside of the body at $y = 0$ plane.

CONCLUSIONS

Large eddy simulations (LES) are performed to study the characteristics of flow over a 6:1 spheroid placed at an angle of incidence $\alpha = 10°$. We present results at $Re = 5 \times 10^3$ and $Fr = \infty, 6, 1.9$, and 1. Additionally, flows past a 6:1 spheroid at the same (Re, Fr) combinations but at $\alpha = 0°$ are simulated to provide a basis for comparison. We find that the buoyancy effect introduced by stratification strongly modulates the pressure and friction forces on the body. The critical Froude number (Ortiz-Tarin *et al.*, 2019) given by $Fr_c = L/\pi D$ is defined kinematically by equating the body length to the half-wavelength of the generated lee wave. For the 6:1 spheroid, the effect of stratification on C_p, C_f, and C_d is more pronounced at $Fr = 1$ than at the critical Froude number $Fr_c \approx 1.9$. For both $\alpha = 0°$ and $10°$ cases, C_d monotonically increases with decreasing Fr. At $\alpha = 10°$, a distinct lateral asymmetry is visible in the C_p and C_f contours for $Fr = 6$ and ∞ cases. This gives rise to a non-zero lateral force whose magnitude is approximately 12% of the streamwise drag at $\alpha = 10°$. Further increasing the stratification kills the asymmetry at $Fr = 1.9$ and 1. At $\alpha = 10°$, we also find that the flow separation over the body is strongly dependent on the value of Fr. At $Fr = 6$ and ∞, the flow separates from the lateral sides on the lee of the body while at $Fr = 1$, the flow separates predominantly near the vertical center plane $y = 0$. In the future studies, we plan to investigate flow separation and topology of shed vortices and their potential link to the flow asymmetry in $\alpha = 10°$ cases as well as wake dynamics.

ACKNOWLEDGEMENTS

We gratefully acknowledge the support of the Office of Naval Research grant N0014-20-1-2253.

REFERENCES

Ashok, A., Van Buren, T. & Smits, A. J. 2015*a* Asymmetries in the wake of a submarine model in pitch. *J. Fluid Mech.* **774**, 416–442.

Ashok, A., Van Buren, T. & Smits, A. J. 2015*b* The structure of the wake generated by a submarine model in yaw. *Exp Fluids* **56** (6), 123.

Bonneton, P., Chomaz, J. M. & Hopfinger, E. J. 1993 Internal waves produced by the turbulent wake of a sphere moving horizontally in a stratified fluid. *J. Fluid Mech.* **254**, 23–40.

Chesnakas, C.J. & Simpson, R.L. 1994 Full three-dimensional

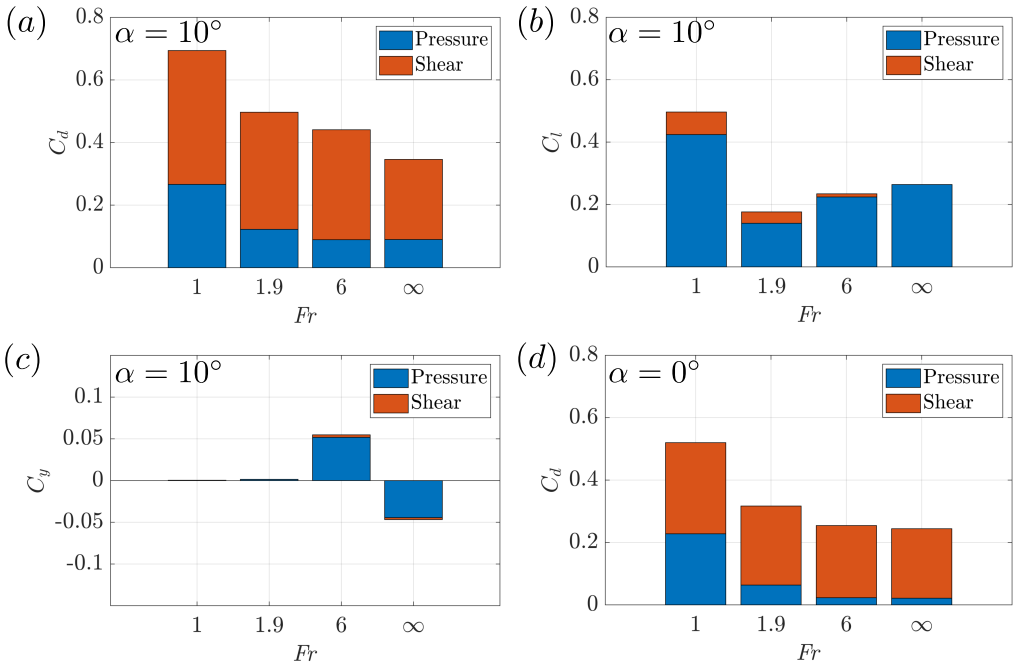

Figure 4: Force coefficients decomposed between pressure and shear contribution: (a) coefficient of drag C_d, (b) coefficient of lift C_l, (c) lateral force C_y at $\alpha = 10°$, and (d) C_d at $\alpha = 0°$.

measurements of the cross-flow separation region of a 6: 1 prolate spheroid. *Exp. Fluids* **17** (1), 68–74.

Chevray, R. 1968 The turbulent wake of a body of revolution. *J. Basic Eng* pp. 275–284.

Chongsiripinyo, K. & Sarkar, S. 2019 Decay of turbulent wakes behind a disk in homogeneous and stratified fluids. *J. Fluid Mech.* **885**, A31.

Constantinescu, G. S., Pasinato, H., Wang, Y., Forsythe, J. R. & Squires, K. D. 2002 Numerical investigation of flow past a prolate spheroid. *J. Fluids Eng.* **124** (4), 904–910.

Dalla Longa, L., Evstafyeva, O. & Morgans, A. S. 2019 Simulations of the bi-modal wake past three-dimensional blunt bluff bodies. *J. Fluid Mech.* **866**, 791–809.

Fu, T.C., Shekarriz, A., Katz, J. & Huang, T.T. 1994 The flow structure in the lee of an inclined 6: 1 prolate spheroid. *J. Fluid Mech.* **269**, 79–106.

Grandemange, M., Gohlke, M. & Cadot, O. 2013 Turbulent wake past a three-dimensional blunt body. Part 1. Global modes and bi-stability. *J. Fluid Mech.* **722**, 51–84.

Han, T. & Patel, V. C. 1979 Flow separation on a spheroid at incidence. *J. Fluid Mech.* **92** (4), 643–657.

Jiang, F., Gallardo, J. P., Andersson, H. I. & Zhang, Z. 2015 The transitional wake behind an inclined prolate spheroid. *Phys. Fluids* **27** (9), 093602.

Jiménez, J. M., Hultmark, M. & Smits, A. J. 2010 The intermediate wake of a body of revolution at high Reynolds numbers. *J. Fluid Mech.* **659**, 516–539.

Kumar, P. & Mahesh, K. 2018 Large-eddy simulation of flow over an axisymmetric body of revolution. *J. Fluid Mech.* **853**, 537–563.

Meunier, P., Le Dizès, S., Redekopp, L. & Spedding, G. R. 2018 Internal waves generated by a stratified wake: experiment and theory. *J. Fluid Mech.* **846**, 752–788.

Nidhan, S., Chongsiripinyo, K., Schmidt, O. T. & Sarkar, S. 2020 Spectral proper orthogonal decomposition analysis of the turbulent wake of a disk at re= 50 000. *Phys. Rev. Fluids* **5** (12), 124606.

Nidhan, S., Ortiz-Tarin, J. L., Chongsiripinyo, K., Sarkar, S. & Schmid, P. J. 2019 Dynamic Mode Decomposition of Stratified Wakes. In *AIAA Aviation 2019 Forum*. Dallas, Texas: American Institute of Aeronautics and Astronautics.

Nidhan, S., Schmidt, O.T. & Sarkar, S. 2022 Analysis of coherence in turbulent stratified wakes using spectral proper orthogonal decomposition. *J. Fluid Mech.* **934**.

Ortiz-Tarin, J.L., Nidhan, S. & Sarkar, S. 2021 High-reynolds-number wake of a slender body. *J. Fluid Mech.* **918**.

Ortiz-Tarin, J. L., Chongsiripinyo, K. C. & Sarkar, S. 2019 Stratified flow past a prolate spheroid. *Phys. Rev. Fluids* **4** (9), 094803.

Patel, V.C. & Kim, S.E. 1994 Topology of laminar flow on a spheroid at incidence. *Comp. Fluids* **23** (7), 939–953.

Piquet, J. & Queutey, P. 1992 Navier-stokes computations past a prolate spheroid at incidence - I. Low incidence case. *Comp. Fluids* **21**, 599–625.

Posa, A. & Balaras, E. 2016 A numerical investigation of the wake of an axisymmetric body with appendages. *J. Fluid Mech.* **792**, 470–498.

Rigas, G., Oxlade, A. R., Morgans, A.S. & Morrison, J. F. 2014 Low-dimensional dynamics of a turbulent axisymmetric wake. *J. Fluid Mech.* **755**, R5.

Tezuka, Asei & Suzuki, Kojiro 2006 Three-Dimensional Global Linear Stability Analysis of Flow Around a Spheroid. *AIAA Journal* **44** (8), 1697–1708.

Wang, K.C., Zhou, H.C., Hu, C.H. & Harrington, S. 1990 Three-dimensional separated flow structure over prolate spheroids. *Proc. R. Soc. A: Math. Phys. Eng. Sci.* **429** (1876), 73–90.

Wikström, N., Svennberg, U., Alin, N. & Fureby, C. 2004 Large eddy simulation of the flow around an inclined prolate spheroid. *J. Turbul.* **5** (1), 029.